Additive Manufacturing Letters 15 (2025) 100316

Contents lists available at ScienceDirect

Additive Manufacturing Letters

journal homepage: www.elsevier.com/locate/addlet

Short Communication

Load direction and temperature impacts on cyclic creep behavior of laser-based powder bed fusion-produced WE43 magnesium alloy

Alexander Koch [a,*], Sebastian Stammkoetter [a], Arvid Abel [b], Abootorab Chehreh [a], Joerg Hermsdorf [b], Stefan Kaierle [b], Frank Walther [a]

[a] TU Dortmund University, Chair of Materials Test Engineering (WPT), Baroper Str. 303, 44227 Dortmund, Germany
[b] Laser Zentrum Hannover e.V., Hollerithallee 8, 30419 Hannover, Germany

ARTICLE INFO

Keywords:
Magnesium alloy WE43
Additive manufacturing
Laser-based powder bed fusion (PBF-LB/M)
Fatigue testing
(Cyclic) creep behavior
Elevated temperature

ABSTRACT

Magnesium alloys are renowned for their high strength-to-weight ratio and low density, making them highly sought-after in the lightweight engineering sector. Among these, the high-strength magnesium alloy WE43, characterized by its Mg-4Y-3RE composition, stands out for its superior mechanical strength and thermal stability. These properties, coupled with its creep resistance, render WE43 a suitable alloy in elevated temperature applications, particularly in aerospace and automotive engineering. Despite its potential, the characterization of the load direction- and temperature-dependent deformation behavior remains incomplete for WE43, especially in additive manufacturing contexts. This study explores the quasi-static and cyclic creep properties of WE43 produced via laser-based powder bed fusion.

The research involved tensile and compression testing to evaluate quasi-static deformation and tensile-compression asymmetry. Cyclic creep behavior was studied under diverse mechanical (tension, compression) and thermal (RT, 200 °C, 300 °C) conditions by load-increase fatigue tests. Microstructural analyses based on cross-sections, XRD and computed tomography were conducted to assess manufacturing quality and identify potential inhomogeneities. The results reveal the interplay between mechanical load, temperature, and structural integrity in WE43. It could be shown that especially at 300 °C increased creep rates occure.

1. Introduction

Magnesium alloys, particularly WE43, have garnered significant attention in engineering applications due to their high strength-to-weight ratio and low density. WE43, composed primarily of magnesium with additions of yttrium, neodymium, gadolinium, and zirconium, exhibits notable mechanical strength and, compared to other Mg alloys, high thermal stability and creep resistance, making it suitable for elevated temperature environments such as aerospace and automotive industries [1,2].

Traditional manufacturing methods for magnesium alloys, including casting and extrusion, often face limitations in design flexibility and may result in microstructural inhomogeneities, e.g. pores, that may affect mechanical performance. The different production methods can induce significant anisotropy due to directional solidification or deformation patterns. In casting, directional solidification leads to the formation of dendritic grain structures, porosity, and chemical segregation. The dendrites grow preferentially along thermal gradients, introducing anisotropy in both mechanical properties and defect distribution. Additionally, porosity tends to localize along interdendritic regions, where solute-enriched zones resist proper feeding during solidification [3,4]. In extrusion, intense plastic deformation along the extrusion axis elongates grains and aligns crystallographic basal planes, resulting in pronounced anisotropy. This causes strong directionality in mechanical behavior (e.g., yield strength, ductility, fatigue) due to the texture-dependent activation of slip and twinning in the HCP structure of magnesium [5]. Even additive manufacturing methods such as laser-based powder bed fusion (PBF-LB/M), though offering high geometrical freedom, introduce their own types of anisotropy. The layer-wise build-up and rapid thermal gradients lead to columnar grain growth aligned with the build direction and potential interlayer porosity. This structural orientation causes directional mechanical behavior and tension-compression asymmetry in the final parts [6]. Especially for magnesium challenges exist due to the poor weldability

* Corresponding author.
E-mail address: alexander3.koch@tu-dortmund.de (A. Koch).

https://doi.org/10.1016/j.addlet.2025.100316
Received 30 May 2025; Received in revised form 4 August 2025; Accepted 11 August 2025
Available online 11 August 2025

properties [7]. The aforementioned limitations restrict the potential of magnesium alloys in advanced applications, where uniformity and defect-free structures are critical. PBF-LB/M allows for the fabrication of complex geometries with the potential of precise control over microstructure and mechanical properties by adjusting process parameters such as laser power, scan speed, and layer thickness [8–10]. Moreover, recent process controls have reduced porosity and oxidation issues [8,11,12]. Despite these advancements, further optimization of AM parameters is essential to produce defect-free components with adequate microstructure and anisotropy for critical applications.

Creep behavior in WE43 is strongly temperature- and stress-dependent. At lower temperatures and stress levels, creep deformation is dominated by dislocation motion and precipitate interactions, which effectively resist deformation [13,14]. However, as temperatures rise, diffusion-based mechanisms, such as lattice diffusion (Nabarro-Herring creep) and grain boundary diffusion (Coble creep), become more prominent [15–17]. These mechanisms allow atoms to migrate through the crystal lattice or along grain boundaries, leading to time-dependent deformation [18,19].

The transition from dislocation-controlled to diffusion-controlled creep is often observed in WE43 at temperatures approaching 300 °C, corresponding to the onset of precipitate coarsening and grain boundary weakening. Grain boundary sliding becomes a significant factor in this regime, especially in fine-grained structures, which are more susceptible to this type of deformation [20,21]. Moreover, the applied stress level influences the activation of these mechanisms. At high stresses, dislocation climb becomes dominant, while at lower stresses, diffusion and grain boundary sliding prevail [19,22].

Additive manufacturing (AM) enables precise control over material microstructure and the production of complex geometries, but it introduces specific challenges for creep resistance. AM-produced materials often exhibit unique microstructural features, such as fine grains, anisotropic textures, porosity, and residual stresses caused by rapid cooling and localized heat inputs [23,24]. These characteristics can either enhance or impair creep behavior depending on the material and loading conditions [25,26]. For magnesium alloys such as WE43, the hexagonal close-packed (HCP) crystal structure limits dislocation activity, making the alloy inherently prone to grain boundary sliding [27,28]. However, the homogeneous distribution of precipitates improves creep resistance by pinning dislocations. Post-processing treatments, like hot isostatic pressing (HIP), are often employed to reduce porosity and improve the high-temperature stability of AM-produced components. Materials with fine grains or a high fraction of grain boundaries are particularly susceptible to cyclic creep due to the promotion of grain boundary sliding and crack initiation [29].

WE43′s biocompatibility enables its use in bioresorbable AM implants, where cyclic creep resistance is critical, which can be reduced by RE-containing Mg alloys [30,31].

In such biomedical scenarios, the primary loading is cyclic and multiaxial, often arising from walking or muscle movement. Creep deformation under these conditions typically occurs as cyclic (ratcheting) creep, where a small plastic strain accumulates per cycle even at stress levels below the yield strength [30]. Typical operating conditions for biodegradable magnesium implants involve body temperature (~37 °C), stress amplitudes of 5–30 MPa, and load frequencies between 0.5–3 Hz, depending on location and patient activity [32,33]. While classical steady-state (constant-stress) creep is minimal at these temperatures, cyclic creep becomes a key degradation mode over weeks to months due to repeated physiological loading [33]. Therefore, understanding the load-direction- and temperature-dependence of cyclic creep is essential to predict long-term implant performance and avoid premature loss of mechanical integrity. This study specifically investigates the material response under such repeated loading conditions, and thus focuses on the mechanisms of cyclic creep, rather than traditional constant-load creep.

The alloy's ability to be processed via AM facilitates the creation of patient-specific geometries, potentially reducing the need for secondary surgeries [34]. However, a critical aspect of its biomedical application is the control of creep to maintain mechanical integrity throughout the healing process.

Key challenges include optimizing AM processing and alloy composition to ensure defect-free, homogeneous structures and cost-efficiency. This includes refining process parameters, such as laser power and scan speed, and improving powder quality to achieve consistent results. The aim of this paper is to address these gaps by systematically investigating the creep behavior of additively manufactured WE43 magnesium alloy, particularly under quasi-static and cyclic loading at elevated temperatures. The investigations seek to correlate microstructural features with deformation mechanisms and explore the implications of these findings for high-temperature applications. The results will clarify the mechanisms of static and cyclic creep to enhance the performance and reliability of WE43 in demanding operational conditions.

2. Experimental procedure

2.1. Material

The experimental investigation focusses on exploring the quasi-static and cyclic creep behavior of WE43 magnesium alloy, which was additively manufactured using laser-based powder bed fusion (PBF-LB/M). The powder was delivered by New Materials Development GmbH (Rosenheim, Germany). WE43 was chosen due to its high mechanical strength, creep resistance, and thermal stability, making it an ideal candidate for elevated temperature applications. The alloy, primarily composed of magnesium with rare earth elements such as yttrium, neodymium, gadolinium, and zirconium, exhibits a balance of mechanical properties suitable for demanding aerospace, automotive, and biomedical applications. However, its high sensitivity to temperature and manufacturing conditions necessitated a detailed investigation of its behavior under different thermal and mechanical loads. 97.3 % of the particles exhibit a grain size ⟨ 53 µm and 2.7 % a grain size ⟩ 53 µm. The chemical composition of the powder is given in Table 1.

2.2. Additive manufacturing process

Additive manufacturing was performed using the PBF-system SLM 125HL by Nikon SLM Solutions. The WE43 powder underwent preprocessing to ensure its quality. The powder, with a particle size range of 15 to 53 µm, displayed a spherical morphology with minimal agglomeration. The elemental composition included yttrium, neodymium, gadolinium, and zirconium, forming a robust microstructure upon solidification. Scanning electron microscopy (Fig. 1) confirmed the powder's suitability for the PBF-LB/M process, since a homogeneous size distribution with round particles is evident.

The additive manufacturing process was carried out using a 100 W yttrium fiber laser. A preheating temperature of 200 °C was applied to the build plate to reduce residual stresses, while the laser power, scan speed, and hatch distance were systematically varied to identify optimal processing parameters. The manufacturing trials revealed significant dependencies of porosity and mechanical quality on the laser parameters and the positional placement of specimens on the build plate. Fig. 2b shows the microstructure of as-build additive manufactured WE43 specimens with conventional specimen design (Fig. 2a) containing several cracks in the surface areas and significant porosity in the inner areas due to the thermal conditions in the material and the non-optimized scanning strategy.

Table 1
Chemical composition of WE43 magnesium powder (in wt %).

	Y	Gd	Nd	Zr	Fe	Zn	Mg
Powder	3.76	1.24	2.47	0.40	0.01	0.21	Bal.

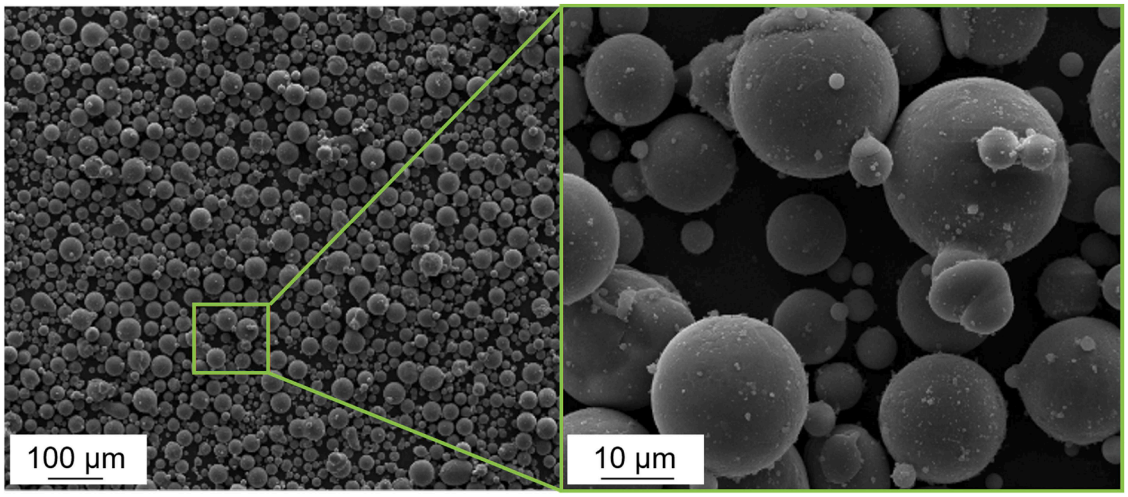

Fig. 1. SEM image of the WE43 alloy powder [10].

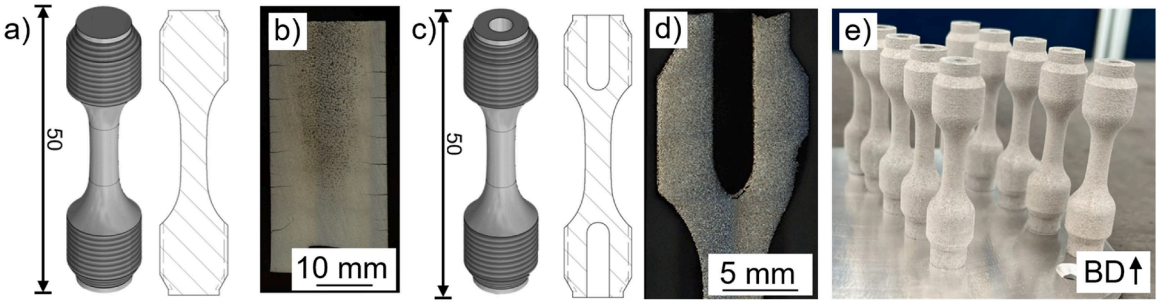

Fig. 2. Initial specimen geometry for tensile and fatigue investigations (a) with subsequent crack and pore containing cross-sections (b), adopted specimen geometry with blind holes at front sides (c) with subsequent nearly crack free and negligible pore containing microstructure (d), additively manufactured WE43 alloy specimens on the build platform (e), BD: build direction.

To identify suitable manufacturing parameters, a series of preliminary trials was performed (see Supplementary material A). Based on these results, the final process parameters were selected to minimize porosity and maximize mechanical properties of the samples. The optimization process of the process parameters using the adopted geometry led to a laser power of 75 W, a scanning speed of 300 mm/s, a hatch distance of 60 µm, a layer height of 40 µm and a defocusing of 2.5 mm.

2.3. Specimen design

To address the aforementioned initial challenges with porosity and near-surface cracks in the manufactured specimens, the design of the tensile specimens was iteratively optimized. Initial geometries (Fig. 2a) suffered from cracks and excessive porosity (Fig. 2b), particularly in the top layers, where thermal gradients were most pronounced. To mitigate these issues, a blind hole was introduced into the upper and lower ends of fatigue specimens (Fig. 2c), effectively reducing heat accumulation and enhancing thermal uniformity during the build process. In addition, the scanned area was reduced by this strategy in order to minimize the addition of thermal stresses. Microstructural analyses and subsequent metallography (Fig. 2d) as well as X-ray computed tomography (CT) scans (chapter 3.1) confirmed that the final specimens (Fig. 2e) achieved near-complete density with negligible porosity and without cracks. Post-processing of the fabricated specimens involved mechanical detachment from the build plate, followed by precision grinding and polishing to prevent influences of surface roughness.

2.4. Metallography and microscopy

The microstructural analysis of the WE43 magnesium alloy was conducted using light microscopy to examine the grain structure, precipitate distribution, and surface quality. The samples were embedded in a conductive mounting resin to provide stability during polishing and imaging. A sequential polishing process was employed, beginning with coarse grinding using silicon carbide papers of progressively finer grit sizes, followed by polishing with diamond suspensions (3 µm and 1 µm) to achieve a mirror-like surface. The final step involved vibratory polishing with colloidal silica to remove any residual surface deformation and scratches, allowing for a detailed view of microstructural features.

All optical microscopy images were captured using a Keyence VK-X1000, equipped with a high-resolution digital camera and advanced illumination settings for enhanced contrast. In order to identify the melt pools within the microstructure, the specimens shown in Fig. 4 were etched using nitric acid with a concentration of 3 %.

2.5. Residual stress measurement

In order to identify the occurring phases, XRD (X-ray diffraction) measurements were performed using a Bruker D8 Discover diffractometer. In the context of phase analyses, diffractograms were taken using the parameters given in Table 2. The specimens were ground and polished as described in chapter 2.4 prior to the XRD measurements. The diffractometer was equipped with Cu Kα radiation ($\lambda = 1.5406$ Å). The scans were performed in Bragg–Brentano geometry over a 2θ range of 19°–81°, with a step size of 0.05° and a counting time of 7.5 s/step.

Measurements were carried out on the XY plane (perpendicular to

Table 2
Parameters for XRD investigations.

Parameter	Unit	Value	Parameter	Unit	Value
Target	–	Cu	Wave length k-α_1	Å	1.54
Bragg angle 2Θ		19–81	Voltage V	kV	40
Collimator Ø	mm	0.3	Current I	mA	40
Step size		0.05	Dwell time	s	7.5

the build direction), corresponding to the layering direction of the PBF-LB/M process. This orientation allows for evaluating texture-related phase visibility and comparing dominant phases aligned with the layer plane. The obtained diffraction peaks were indexed using ICDD database references for hexagonal Mg, Mg_3Gd, and Y_2O_3. The presence of Y_2O_3 has also been reported in other studies on PBF-LB/M-produced WE43 [6], and is attributed to residual oxygen in the build chamber atmosphere reacting with yttrium during laser melting.

2.6. Computed tomography

In addition to the metallographic investigations of the microstructure, the defect structure was characterized by means of X-ray computed tomography (CT) using a Nikon XT H 160 system. For all tensile and compression specimens a scan power of 15 W, a current of 150 mA and a voltage of 100 kV was used, leading to an achieved resolution of 9 µm. The computed tomography scans, analyzed using VGStudio Max 2.2 software, quantified the size, shape, and volume of internal defects.

2.7. Quasi-static characterization

Quasi-static mechanical testing was conducted to characterize differences between tension and compression load direction on additively manufactured WE43 alloy. Tensile and compression tests were performed at room temperature (RT), 200 °C, and 300 °C. These tests measured the stress-strain response of the alloy under quasi-static loading conditions and provided the temperature-dependent mechanical properties. The tests were carried out strain-controlled using a Schenck PC63M with Instron 8800 electronics servohydraulic testing system with a strain rate of $\dot{\varepsilon} = 0.00025\ s^{-1}$ in the elastic region ($\varepsilon_t < 1$ %) and $\dot{\varepsilon} = 0.0067\ s^{-1}$ in the elastic-plastic region ($\varepsilon_t > 1$ %). For the control of the strain, a Sandner extensometer with ceramic knifes was used. The test setup for quasi-static as well as cyclic investigations in depicted in Fig. 3a.

The tensile specimens (Fig. 3b) were build based on the geometry optimization during the AM process. Compression specimens (Fig. 3c) were machined as rods to ensure parallel end faces and uniform dimensions.

2.8. Cyclic characterization

The cyclic investigations were carried out in order to evaluate the alloy's performance under repeated mechanical loading, particularly its creep behavior in tensile and compressive conditions. For a rapid qualification of the cyclic properties, load increase tests (LIT) were conducted, during which the load is increased (tension-tension) or decreased (compression-compression) in every cycle up to the failure of the specimen (see [35,36]) The tests were conducted using the identical servohydraulic testing system equipped with high-temperature extensometer compared to the quasi-static tests. Specimens were subjected to cyclic loading at a frequency of $f = 10$ Hz and a stress amplitude of $\sigma_a = 4.5$ MPa. The tests were carried out at RT, 200 °C, and 300 °C to simulate realistic operational conditions. Due to the high complexity and resource requirements of producing defect-free magnesium specimens for multiple testing conditions using PBF-LB/M, this study focused on representative single samples per condition for quasi-static as well as cyclic characterization.

3. Results and discussion

3.1. Microstructure and defect structure

The microstructural investigations of the additively manufactured WE43 specimens (Fig. 4) reveal a highly dense material structure, with computed tomography (CT) scans (Fig. 6) confirming a density of 99.5 % across the optimized specimens. Isolated defects are detected, predominantly in the peripheral regions of the build plate. These results align with studies highlighting the sensitivity of PBF-LB/M to spatial thermal and smoke variations, which can exacerbate porosity and defect formation when process parameters are not adequately controlled [8,37].

The light microscopy images show a typical macrostructure for additively manufactured material with clearly visible melt pools containing small circular grains (about 3.7 ± 2.5 µm), determined by means of EBSD (EDAX Super Velocity in a Tescan MIRA 3 SEM, 15 kV acceleration voltage, beam intensity 12, step size 50 nm) and aligned grains based on the laser pathways. It gets clear that the optimized specimens exhibit a fine-grained microstructure with well-dispersed precipitates, especially at the grain boundaries. These secondary phases, determined in detail by the XRD measurements (Fig. 5) play a critical role in impeding dislocation movement and enhancing creep resistance at

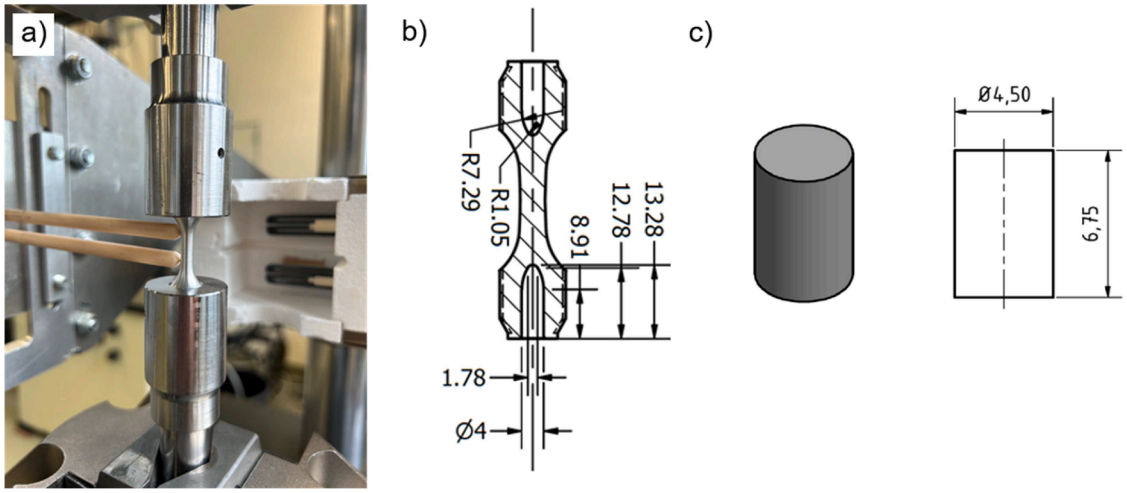

Fig. 3. Test setup for quasi-static and cyclic investigations under high temperature (a), specimen geometry for tensile tests and tension-tension fatigue tests (b), specimen geometry for compression tests and compression-compression fatigue tests (c), dimensions in mm.

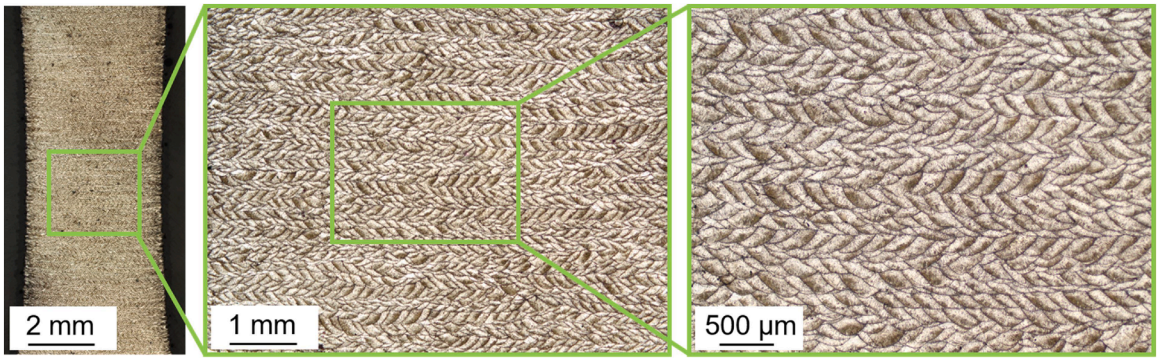

Fig. 4. Metallographic images of additively manufactured WE43 magnesium alloy.

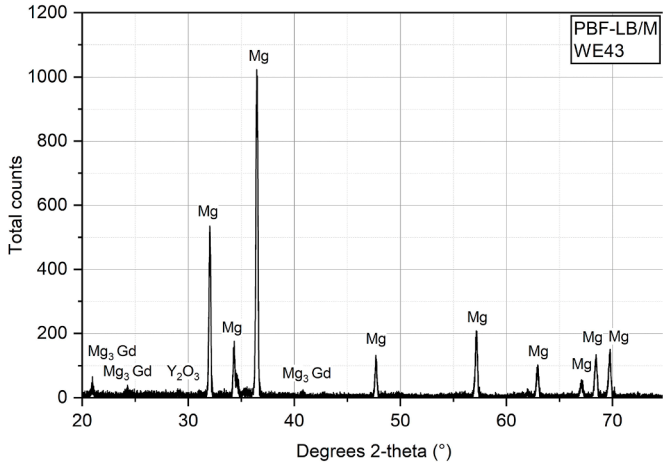

Fig. 5. Diffraction pattern gained by XRD measurements for phase analysis.

elevated temperatures. The uniform distribution of these precipitates is consistent with prior studies, which emphasize the importance of thermal stability in rare-earth-containing magnesium alloys for their high-temperature applications [6,8]. Additionally, grain boundary formation indicates minimal sliding activity, confirming that the PBF-LB/M process, under optimized parameters, can produce specimens with superior microstructural integrity.

The X-ray diffraction (XRD) analysis (Fig. 5) reveals a microstructural composition predominantly characterized by α-Mg as the primary phase, accompanied by the secondary phases Mg_3RE (Mg_3Gd) and Y_2O_3. The diffraction peaks corresponding to magnesium (Mg) exhibit strong intensities, confirming the presence of a hexagonal close-packed (HCP) structure as the matrix phase. The presence of Mg_3Gd precipitates indicates the formation of intermetallic compounds that are known to contribute to the strengthening of the alloy through precipitation hardening mechanisms, as also reported in conventionally processed WE43 alloys [38,39]. Additionally, the detection of Y_2O_3 suggests the presence of yttrium-based oxide inclusions, which may form due to oxygen affinity during the laser powder bed fusion process, as observed in prior studies on rare-earth-containing magnesium alloys [40].

Compared to conventionally cast WE43 alloys, which typically exhibit larger and more dispersed intermetallic precipitates due to slower cooling rates [5], the XRD results confirm that the additive manufacturing process promotes refined microstructural features, likely leading to enhanced mechanical properties [41]. The formation of Mg_3Gd precipitates aligns with previous reports indicating that rare-earth elements, particularly gadolinium, effectively strengthen magnesium alloys by refining the microstructure and impeding dislocation movement [42]. Moreover, the relatively sharp and well-defined diffraction peaks suggest a high degree of crystallinity, which is essential for maintaining mechanical integrity under cyclic and creep loading conditions.

The presence of Y_2O_3 phases, while beneficial for oxidation resistance, may also influence mechanical properties by affecting grain boundary cohesion. Prior studies have indicated that oxide particles at grain boundaries can serve as crack initiation sites during cyclic loading, potentially impacting fatigue performance [43]. However, under compression-dominated loading conditions, such oxides can contribute to enhanced creep resistance by restricting grain boundary sliding, a critical deformation mechanism at elevated temperatures [44].

The computed tomography (CT) reconstructions (Fig. 6) reveal comparatively few defects, indicating a high-quality laser-based powder bed fusion (PBF-LB/M) process. However, a notable observation is the orientation of these defects, which appear predominantly aligned perpendicular to the loading direction. This orientation of the defects, evaluated based on the difference of the projected area in and perpendicular to the build direction suggests that the pores are located at the interfaces between individual layers during the additive manufacturing process, where incomplete fusion or insufficient thermal bonding may have occurred (lack of fusion porosity). Such inter-layer defect distribution is characteristic of AM processes and has been similarly observed in studies of other metallic alloys produced via PBF-LB/M [45,46].

The defect size and frequency observed are significantly reduced compared to conventionally manufactured AM components, where porosity levels can reach up to 2–3 % under non-optimized conditions. In the present case, the defects are small, sparse, and isolated, suggesting an overall porosity below 0.5 %, which therefore can be treated as nearly dense. This low porosity aligns with the optimization of process parameters, such as laser power, scan speed, and hatch distance, and especially the geometrical optimization described in chapter 2, to achieve near-full density, as highlighted in previous studies on magnesium alloys. For comparison, work by Liu et al. [47] on additively manufactured metals demonstrates that minimizing inter-layer porosity directly improves strength and fatigue resistance, as fewer defects act as crack initiation sites under mechanical, especially cyclic loading.

While this low porosity supports improved mechanical properties, the orientation of remaining defects, especially inter-layer pores perpendicular to the loading direction, may locally reduce tensile strength and fatigue life due to enhanced grain boundary sliding and early crack initiation under cyclic or high-temperature loading. In addition, this defect orientation is particularly relevant for creep behavior, as inter-layer voids can act as pathways for grain boundary sliding and void coalescence under sustained high-temperature stresses.

3.2. *Quasi-static behavior*

The quasi-static mechanical behavior of additively manufactured WE43 specimens reveals a distinct anisotropy between tensile (Fig. 7a) and compressive (Fig. 7b) loading conditions at all investigated temperatures - room temperature (RT), 200 °C and 300 °C. This anisotropy

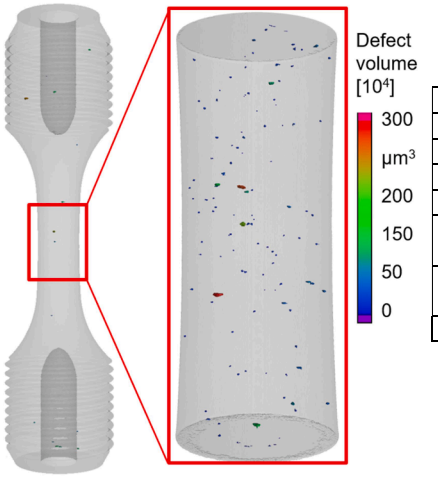

Number of defects	235
Investigated volume (mm³)	134
Porosity (%)	0.47
Defect diameter (µm)	63 ± 15
Shape factor	0.67 ± 0.24
Projected defect area in build direction (µm²)	56 ± 20
Projected defect area perpendicular to build direction (µm²)	37 ± 18
Equivalent defect diameter (µm)	43 ± 15

Fig. 6. Volume reconstruction of additively manufactured WE43 specimens with characteristic defect parameters.

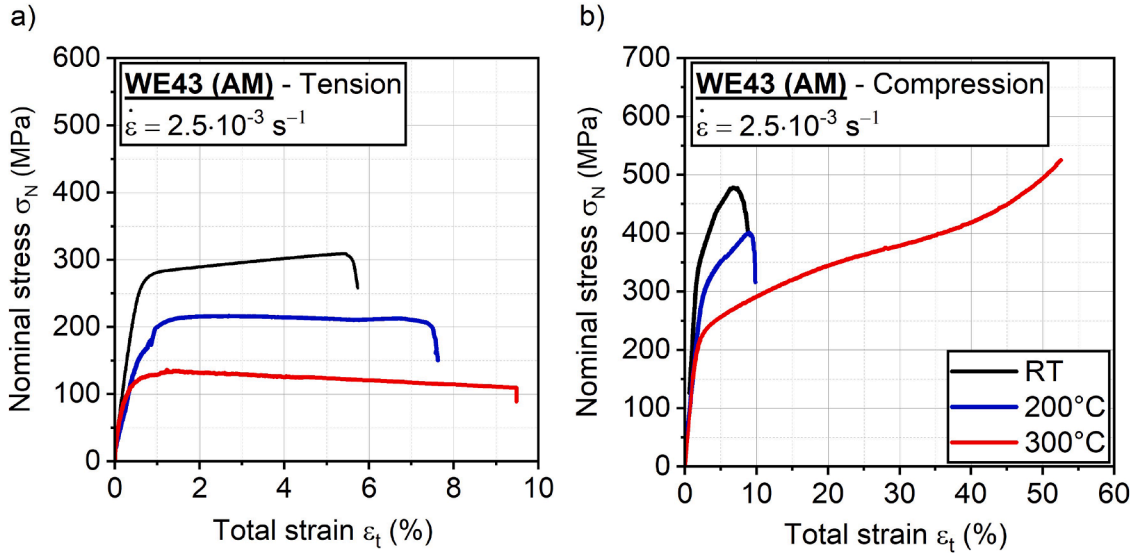

Fig. 7. Quasistatic tensile (a) and compression (b) tests of additively manufactured WE43 alloy at room temperature (RT), 200 °C and 300 °C.

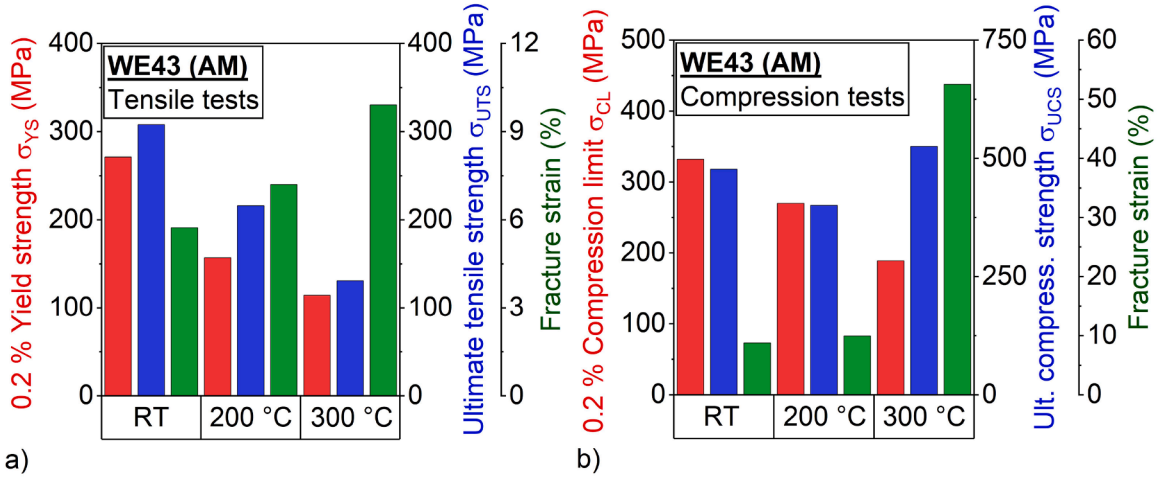

Fig. 8. Tensile (a) and compression (b) properties of additively manufactured WE43 alloy.

arises primarily from microstructural characteristics, stress-state-dependent deformation mechanisms, and the inherent features of the additive manufacturing (AM) process. Fig. 8a (tensile) and Fig. 8b (compression) represent the evaluated yield strength/compression limit, ultimate tensile/compression strength and fracture strain.

At room temperature, the tensile yield strength reaches approximately 270 MPa, with an ultimate tensile strength (UTS) of around 310 MPa and a fracture strain of about 6 %. In contrast, under compressive loading, the yield strength is higher at 330 MPa, which is consistent with the expected asymmetry in tension-compression response of magnesium alloys due to twinning mechanisms [43,48,49]. The ultimate compressive strength exceeds 470 MPa and a significantly larger fracture strain of 9 %. Tensile failure occurs earlier due to the alignment of inter-layer defects, which are inherent to the AM process, perpendicular to the loading direction. These defects, including small voids and incomplete fusion zones, act as stress concentrators under tensile stresses, promoting early crack initiation and propagation. In compression, these same defects are less critical, as the compressive forces close voids rather than propagate cracks.

At 200 °C, the anisotropy between tension and compression persists. The tensile yield strength drops to approximately 160 MPa, with an ultimate tensile strength of 216 MPa, while the fracture strain decreases to about 7 %. This behavior reflects the onset of thermally activated deformation mechanisms, such as dislocation climb and the activation of additional slip systems, which enhance ductility. In compression, the yield strength remains higher at 270 MPa, and the ultimate compressive strength reaches approximately 400 MPa, with the fracture strain increasing to 10 %. This greater ductility under compressive loading arises from the stabilization of grain boundaries and the suppression of crack growth, which further delays failure.

At 300 °C, the anisotropy becomes even more pronounced. Under tensile loading, the yield strength decreases significantly to 115 MPa, with the UTS dropping to approximately 131MPa. The fracture strain, however, increases to around 10 %, reflecting a transition to grain boundary sliding and diffusion-driven creep mechanisms. The compressive stress-strain curve for 300 °C reveals a distinct behavior where no significant drop in nominal stress occurs after reaching the peak value. Instead, the stress continues to increase gradually with ongoing strain (reaching $>$ 52 %), displaying a steady rise in nominal stress throughout the deformation process. This behavior is in contrast to the tensile stress-strain response at the same temperature, where a clear decrease of nominal stress due to necking occurs after the peak value is reached.

The steady increase in nominal stress under compression at elevated temperatures is attributed to the activation of basal slip systems in the HCP structure of magnesium [50]. At 300 °C, thermal activation reduces the critical resolved shear stresses (CRSS) of non-basal systems, enabling dislocation climb and diffusional mechanisms to support plasticity without marked stress softening. This behavior is supported by studies showing enhanced basal slip and constrained grain boundary sliding under compression [51,52]. Li et al. [53] further observed that suppressed tensile stresses at grain boundaries delay strain localization, promoting gradual stress build-up and reduced damage, especially by coalescence and sliding, compared to tension.

Compared to conventionally cast WE43, the additively manufactured material exhibits similar behavior under compression at 300 °C, but benefits from a much finer grain structure (3.8 μm vs. ~38 μm, [37]). This refinement enhances basal slip and dislocation mobility, contributing to the steady stress increase [54,55], while the absence of casting defects delays failure mechanisms like intergranular cracking.

The pronounced anisotropy between tension and compression arises from the layer-wise AM microstructure: elongated grains and inter-layer boundaries aligned perpendicular to the build direction promote failure in tension, whereas compression stabilizes these features and suppresses crack propagation [45]. Additionally, strengthening precipitates contribute to this asymmetry. At low temperatures, they effectively pin dislocations [6], but at 300 °C, coarsening and partial dissolution of precipitations reduce their effect, more so under tension due to grain boundary weakening [13,19].

While AM WE43 outperforms cast material at room temperature (250 – 280 MPa tensile strength) due to refined grains and rapid solidification, both show converging behavior at high temperatures where grain boundary sliding and precipitate coarsening dominate. Nonetheless, AM specimens maintain slightly higher fracture strains at 300 °C, likely due to their defect-free microstructure [18,56].

3.3. Cyclic behavior

The fatigue investigations of additively manufactured WE43 specimens under tensile and compressive loading conditions reveal a behavior influenced by temperature, loading mode, and microstructural mechanisms. Fig. 9 and 10 show the results of the cyclic investigations. σ_a is the stress amplitude. $\varepsilon_{a,p}$ denotes the plastic strain amplitude, i.e., half the difference between the plastic strain at maximum and minimum load. $\varepsilon_{m,t}$ refers to the total mean strain, representing the average of total strain over a load cycle. At room temperature (RT), the material exhibits a stable cyclic behavior in both tension and compression, characterized by minimal plastic strain accumulation and negligible creep effects. Under tensile loading (Fig. 9), the maximum stress increases slightly over the number of cycles, indicating initial cyclic hardening due to dislocation accumulation and interaction. The plastic strain amplitude remains low and stable throughout the fatigue life, and total mean strain does not evolve significantly, reflecting a microstructure that effectively resists damage initiation and crack propagation under cyclic stress at RT.

In compression (Fig. 10), the behavior is similarly stable, with the total mean streain showing a gradual reduction, indicating minimal cyclic softening. The plastic strain amplitude remains nearly constant, demonstrating cyclic hardening effects similar to those in tension. However, under compression, the material achieves a more stable and delayed fatigue response due to the suppression of crack initiation and propagation, as compressive stresses prevent crack propagation and close inter-layer defects and voids, reducing their impact on fatigue performance [57]. At RT, both stress states indicate that the fine-grained microstructure and uniformly distributed precipitates effectively strengthen the material and delay fatigue failure.

At 200 °C, thermally activated mechanisms begin to influence material behavior. Under tensile loading, moderate stress softening and a gradual increase in plastic strain amplitude occur, along with noticeable mean strain evolution, indicating the onset of creep processes like dislocation climb and grain boundary mobility. The curves are comparable to RT. Crack initiation at inter-layer voids and grain boundaries contributes to damage accumulation and softening. In cyclic compression at 200 °C, the material shows greater resistance to degradation. Minimum stress declines slowly, and plastic strain amplitude remains stable until late cycles, reflecting delayed damage. The compressive stress state limits void opening and crack propagation, resulting in slower strain accumulation.

At 300 °C, creep mechanisms dominate. Tension leads to strong softening, a sharp rise in plastic strain amplitude, and rapid mean strain evolution, driven by grain boundary sliding and void coalescence. Precipitate coarsening and grain boundary opening accelerate damage, reducing fatigue life. In contrast, under compression at 300 °C, the plastic strain amplitude increases progressively due to efficient basal slip activation. Grain boundary opening is suppressed, and deformation is governed by dislocation climb and diffusion. Total mean strain rises more gradually, highlighting WE43's superior resistance to compressive fatigue at elevated temperatures.

The comparison between cyclic and quasi-static behavior further emphasizes the impact of stress state and temperature. Under quasi-static loading, the material demonstrates steady deformation under compression at 300 °C due to the activation of basal slip and dislocation mechanisms, whereas tension leads to significant strain softening. In

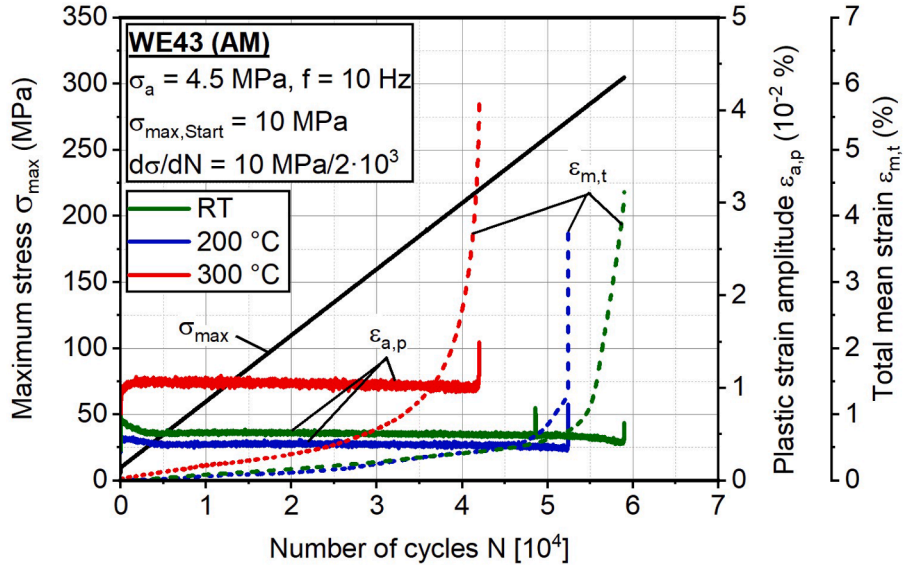

Fig. 9. Load increase test of additively manufactured WE43 alloy in tension-tension loading.

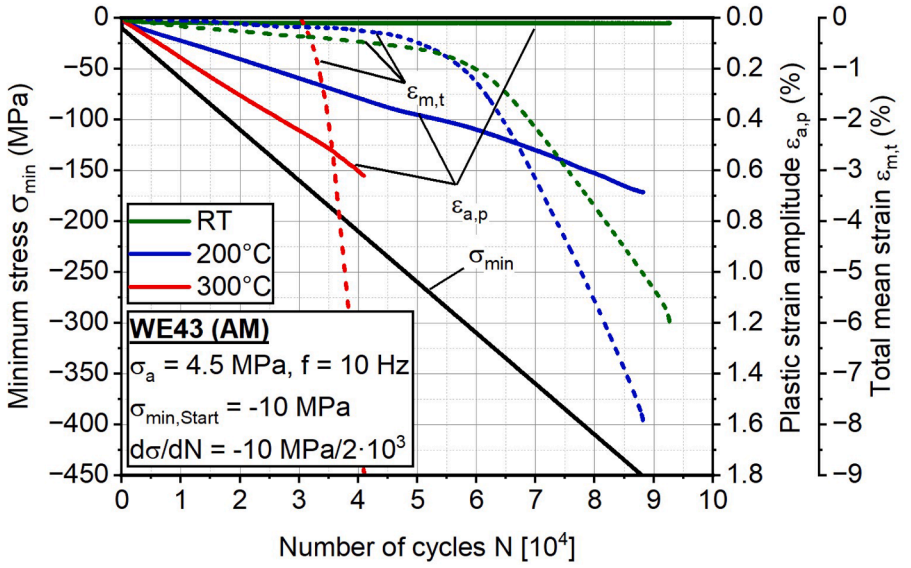

Fig. 10. Load increase test of additively manufactured WE43 alloy in compression-compression loading.

cyclic loading, the repeated stress cycles amplify microstructural damage accumulation, particularly under tensile stresses, where crack initiation and propagation are accelerated. In compression, the suppression of tensile cracks and void growth results in a more gradual accumulation of plastic strain and a longer fatigue life.

When compared to conventionally cast WE43, the additively manufactured material exhibits superior fatigue performance at RT due to its finer grain structure and reduced porosity. Cast materials, which often feature coarser grains and larger defects, are more prone to early crack initiation and fatigue failure. At elevated temperatures, both cast and AM specimens experience reductions in fatigue life due to precipitate coarsening and grain boundary weakening [19]. However, the refined microstructure of AM WE43 may delay these processes, resulting in slightly improved resistance to cyclic creep and better overall performance under compressive loading. Similar trends have been reported in literature for magnesium alloys such as ZK60 and AZ31, where compressive loading consistently results in longer fatigue life compared to tension due to the mitigation of crack initiation and the activation of basal slip systems [48,49].

4. Conclusions and outlook

This study investigated the quasi-static and cyclic creep behavior of the high-performance WE43 magnesium alloy, produced via laser-based powder bed fusion. The results highlighted the intricate relationships between microstructural details, temperature, and loading conditions.

The microstructural analysis revealed that optimized PBF-LB/M processing parameters yielded specimens with near-complete density and well-dispersed precipitates. These microstructural features play an important role in enhancing creep resistance by impeding dislocation motion and stabilizing grain boundaries. However, at elevated temperatures, the coarsening and dissolution of precipitates significantly reduced their effectiveness, leading to grain boundary sliding and accelerated deformation.

Quasi-static tests demonstrated that WE43 retains high strength and low creep rates at room temperature and up to 200 °C, making it suitable

for moderate thermal applications. At 300 °C, the alloy exhibited substantial degradation and activation of additional slip systems, with creep behavior dominated by diffusion mechanisms and grain boundary sliding. These findings align with theoretical models of creep in fine-grained magnesium alloys, emphasizing the importance of microstructural stability in extending the operational temperature range.

Cyclic tests further underscored the alloy's temperature-dependent behavior. At room temperature, cyclic hardening delayed the onset of creep deformation, while at 200 °C, moderate creep strain accumulation reflected a balance between dislocation mobility and precipitate stability for compression. At 300 °C, however, rapid creep strain accumulation and reduced fatigue life occur. The transition from dislocation-mediated mechanisms to grain boundary sliding and void coalescence was evident in both tensile and compression fatigue tests.

These findings underscore the need for alloy design strategies that enhance the thermal stability of WE43, such as optimizing rare earth content or introducing alternative stabilizing elements. For biomedical applications, the study highlighted the importance of controlling creep behavior to ensure the mechanical integrity of resorbable implants, particularly in environments with fluctuating thermal conditions.

Future work should focus on the process development and alloying strategy, especially the adoption of process parameters to reduce porosity and investigate the influence on precipitations. Furthermore, advanced characterization techniques for predictive modeling of creep deformation, and innovative alloying strategies for further enhancement of the material's performance should be taken into account. In further studies, a detailed link to the microstructure by means of fractography and SEM will be delivered. In addition, the use for biomedical applications like implants will be investigated, since magnesium, especially WE43 is a well-suited biomaterial.

CRediT authorship contribution statement

Alexander Koch: Writing – original draft, Visualization, Validation, Supervision, Methodology, Investigation, Data curation, Conceptualization. **Sebastian Stammkoetter:** Writing – review & editing, Visualization, Validation, Methodology, Investigation. **Arvid Abel:** Writing – review & editing, Methodology, Investigation, Conceptualization. **Abootorab Chehreh:** Investigation. **Joerg Hermsdorf:** Writing – review & editing, Supervision, Funding acquisition. **Stefan Kaierle:** Writing – review & editing, Supervision, Funding acquisition. **Frank Walther:** Writing – review & editing, Supervision, Project administration, Funding acquisition, Conceptualization.

Declaration of competing interest

The authors declare that they have no known competing financial interests or personal relationships that could have appeared to influence the work reported in this paper.

Acknowledgements

The authors thank the German Research Foundation (Deutsche Forschungsgemeinschaft, DFG) for its financial support within the research project "Mechanism-oriented characterization of the microstructural and load direction-dependent cyclic creep (ratcheting) behavior of the magnesium alloy WE43" (project no 317233119) as well as the research unit 5250 "Mechanism-based characterization and modeling of permanent and bioresorbable implants with tailored functionality based on innovative in-vivo, in-vitro and in-silico methods" (project no 449916462).

Supplementary materials

Supplementary material associated with this article can be found, in the online version, at doi:10.1016/j.addlet.2025.100316.

Data availability

Data will be made available on request.

References

[1] Z.L. Ning, J.Y. Yi, M. Qian, H.C. Sun, F.Y. Cao, H.H. Liu, J.F. Sun, Microstructure and elevated temperature mechanical and creep properties of Mg–4Y–3Nd–0.5Zr alloy in the product form of a large structural casting, Mater. Des. 60 (2014) 218–225.
[2] B.L. Mordike, Creep-resistant magnesium alloys, Mater. Sci. Eng. A (2002) 103–112.
[3] T. Abbott, M. Easton, C. Caceres, Designing with magnesium: alloys, properties, and casting processes, 2004.
[4] Y. Lu, F. Taheri, M.A. Gharghouri, H.P. Han, Experimental and numerical study of the effects of porosity on fatigue crack initiation of HPDC magnesium AM60B alloy, J. Alloys. Compd. 470 (2009) 202–213.
[5] J. Zhang, S. Han, Y. Sun, X. Chen, P. Chen, Z. Li, G. Huang, et al., Enhanced strength of WE43 magnesium-rare earth alloy via combining extrusion and aging, Mater. Sci. Eng. 880 (2023) 145329.
[6] F. Bär, L. Berger, L. Jauer, G. Kurtuldu, R. Schäublin, J.H. Schleifenbaum, J. F. Löffler, Laser additive manufacturing of biodegradable magnesium alloy WE43: a detailed microstructure analysis, Acta Biomater. 98 (2019) 36–49.
[7] G. Çam, A. Günen, Challenges and opportunities in the production of magnesium parts by directed energy deposition processes, J. Magnes. Alloys 12 (2024) 1663–1686.
[8] H. Hyer, Le Zhou, G. Benson, B. McWilliams, K. Cho, Y. Sohn, Additive manufacturing of dense WE43 Mg alloy by laser powder bed fusion, Addit. Manuf. 33 (2020) 101123.
[9] S. Gangireddy, B. Gwalani, K. Liu, E.J. Faierson, R.S. Mishra, Microstructure and mechanical behavior of an additive manufactured (AM) WE43-Mg alloy, Addit. Manuf. 26 (2019) 53–64.
[10] A. Abel, A. Sharma, H. Holländer, D. Zheng, N. Emminghaus, A. Buling, J. Hermsdorf, et al., PBF-LB of large-area magnesium WE43 structures surface-enhanced by plasma electrolytic oxidation, Prog. Addit. Manuf. 9 (2024) 683–694.
[11] M. Esmaily, Z. Zeng, A.N. Mortazavi, A. Gullino, S. Choudhary, T. Derra, F. Benn, et al., A detailed microstructural and corrosion analysis of magnesium alloy WE43 manufactured by selective laser melting, Addit. Manuf. 35 (2020) 101321.
[12] A. Abel, Y. Wessarges, S. Julmi, C. Hoff, J. Hermsdorf, C. Klose, H.J. Maier, et al., Laser powder bed fusion of WE43 in hydrogen-argon-gas atmosphere, Procedia CIRP. 94 (2020) 21–24.
[13] M. Zha, X. Ma, H.L. Jia, Z.M. Hua, Z.X. Fan, Z.Z. Yang, Y.P. Gao, et al., Dynamic precipitation and deformation behaviors of a bimodal-grained WE43 alloy with enhanced mechanical properties, Int. J. Plast. 167 (2023) 103682.
[14] J.G. Wang, L.M. Hsiung, T.G. Nieh, M. Mabuchi, Creep of a heat treated Mg–4Y–3RE alloy, Mater. Sci. Eng. A (2001) 81–88.
[15] W. Abd-Elaziem, J. Liu, N. Ghoniem, X. Li, Effect of nanoparticles on creep behaviour of metals: a review, J. Mater. Res. Technol. 26 (2023) 3025–3053.
[16] M. Jahedi, B.A. McWilliams, F.R. Kellogg, I.J. Beyerlein, M. Knezevic, Rate and temperature dependent deformation behavior of as-cast WE43 magnesium-rare earth alloy manufactured by direct-chill casting, Mater. Sci. Eng. 712 (2018) 50–64.
[17] Y. Gui, Q. Li, X. Chen, Present development status of anti-creep magnesium rare-earth alloys, Mater. Sci. Eng. 230 (2017) 12014.
[18] C. Xiang, N. Gupta, P. Coelho, K. Cho, Effect of microstructure on tensile and compressive behavior of WE43 alloy in as cast and heat treated conditions, Mater. Sci. Eng.: A 710 (2018) 74–85.
[19] Y.H. Kang, X.X. Wang, N. Zhang, H. Yan, R.S. Chen, Effect of initial temper on the creep behavior of precipitation–hardened WE43 alloy, Mater. Sci. Eng.: A 689 (2017) 419–426.
[20] H. Watanabe, T. Mukai, K. Ishikawa, T. Mohri, M. Mabuchi, K. Higashi, Superplasticity of a particle-strengthened WE43 magnesium alloy, Mater. Trans. (2001) 157–162.
[21] R.K. Sabat, P.K. Samal, M, S. Ahamed, Effect of strain path on the evolution of microstructure, texture and tensile properties of WE43 alloy, Mater. Sci. Eng. 715 (2018) 348–358.
[22] S. Kandalam, R.K. Sabat, N. Bibhanshu, G.S. Avadhani, S. Kumar, S. Suwas, Superplasticity in high temperature magnesium alloy WE43, Mater. Sci. Eng. 687 (2017) 85–92.
[23] W. Chen, B. Yin, K. Li, R. Liao, B. Li, H. Huang, Y. Wu, et al., Superstrengthening effect of beyond-solid-solution laser powder bed fused WE43 magnesium alloy triggered by direct aging treatment, Addit. Manuf. 89 (2024) 104287.
[24] Z. Liu, L. Wang, S. Luo, Y. Feng, S. Zhao, Y. Fu, Effect of heat treatment on microstructure and mechanical properties of WE43 alloy fabricated by wire arc additive manufacturing, Mater. Today Commun. 41 (2024) 110950.
[25] J. Bai, Q. Wang, Z. Men, W. Chen, H. Huang, C. Ji, Y. Li, et al., Generation mechanism of anisotropy in mechanical properties of WE43 fabricated by laser powder bed fusion, Micromachines 15 (2024).
[26] N. Bastola, M.P. Jahan, N. Rangasamy, C.S. Rakurty, A review of the residual stress generation in metal additive manufacturing: analysis of cause, measurement, effects, and prevention, Micromachines. (Basel) 14 (2023).
[27] D.J. Savage, B.A. McWilliams, S.C. Vogel, C.P. Trujillo, I.J. Beyerlein, M. Knezevic, Mechanical behavior and texture evolution of WE43 magnesium-rare earth alloy in

split-Hopkinson pressure bar and Taylor impact cylinder testing, Int. J. Impact. Eng. 143 (2020) 103589.
[28] C. Xiang, Y. Xu, Y. Yang, H. Ding, Z. Wang, Plastic deformation mechanisms and constitutive modeling of WE43 magnesium alloy at various strain rates and temperatures, J. Mater. Res. Technol. 29 (2024) 4110–4128.
[29] Y. Zhang, Q. Huo, Z. Zhang, H. Nagaumi, X. Yang, Analysis on the compressive creep behaviors of Mg–Y alloys with various grain sizes, Mater. Sci. Eng.: A 899 (2024) 146448.
[30] K.F. Farraro, K.E. Kim, S.L.Y. Woo, J.R. Flowers, M.B. McCullough, Revolutionizing orthopaedic biomaterials: the potential of biodegradable and bioresorbable magnesium-based materials for functional tissue engineering, J. Biomech. 47 (2014) 1979–1986.
[31] Y. Chen, Z. Xu, C. Smith, J. Sankar, Recent advances on the development of magnesium alloys for biodegradable implants, Acta Biomater. 10 (2014) 4561–4573.
[32] R.K.S. Raman, S.E. Harandi, Resistance of magnesium alloys to corrosion fatigue for biodegradable implant applications: current status and challenges, Materials 10 (2017) 1316.
[33] S. Amukarimi, M. Mozafari, Biodegradable magnesium-based biomaterials: an overview of challenges and opportunities, MedComm. (2020) 2 (2021) 123–144.
[34] N. Wegner, D. Kotzem, Y. Wessarges, N. Emminghaus, C. Hoff, J. Tenkamp, J. Hermsdorf, et al., Corrosion and Corrosion fatigue properties of additively manufactured magnesium alloy WE43 in comparison to titanium alloy Ti-6Al-4V in physiological environment, Materials (2019) 12.
[35] M. Teschke, A. Koch, F. Walther, Comparison of high-temperature compression and compression-comp ressionFatigue behavior of magnesium alloys DieMag422 and AE42, Materials (2020) 13.
[36] F. Walther, Microstructure-oriented fatigue assessment of construction materials and joints using short-time load increase procedure, Mater. Test. 56 (2014) 519–527.
[37] N.A. Zumdick, L. Jauer, L.C. Kersting, T.N. Kutz, J.H. Schleifenbaum, D. Zander, Additive manufactured WE43 magnesium: a comparative study of the microstructure and mechanical properties with those of powder extruded and as-cast WE43, Mater. Charact. 147 (2019) 384–397.
[38] B. Mordike, T. Ebert, Magnesium, materials science and engineering: a 302 (2001) 37–45.
[39] M.O. Pekguleryuz, A.A. Kaya, Creep resistant magnesium alloys for powertrain applications, Adv. Eng. Mater. 5 (2003) 866–878.
[40] D. Choudhuri, S.G. Srinivasan, M.A. Gibson, Y. Zheng, D.L. Jaeger, H.L. Fraser, R. Banerjee, Exceptional increase in the creep life of magnesium rare-earth alloys due to localized bond stiffening, Nat. Commun. 8 (2017) 2000.
[41] M. Li, F. Benn, T. Derra, N. Kröger, M. Zinser, R. Smeets, J.M. Molina-Aldareguia, et al., Microstructure, mechanical properties, corrosion resistance and cytocompatibility of WE43 Mg alloy scaffolds fabricated by laser powder bed fusion for biomedical applications, Mater. Sci. Eng. C. Mater. Biol. Appl. 119 (2021) 111623.
[42] J.F. Nie, Precipitation and hardening in magnesium alloys, Met. Mater Trans. A 43 (2012) 3891–3939.
[43] A. Chapuis, J.H. Driver, Temperature dependency of slip and twinning in plane strain compressed magnesium single crystals, Acta Mater. 59 (2011) 1986–1994.
[44] M.D. Sangid, H.J. Maier, H. Sehitoglu, The role of grain boundaries on fatigue crack initiation – an energy approach, Int. J. Plast. 27 (2011) 801–821.
[45] N. Sanaei, A. Fatemi, Defects in additive manufactured metals and their effect on fatigue performance: a state-of-the-art review, Prog. Mater. Sci. 117 (2021) 100724.
[46] J. Kluczyński, K. Jasik, J. Łuszczek, B. Sarzyński, K. Grzelak, T. Dražan, Z. Joska, et al., A comparative investigation of properties of metallic parts additively manufactured through MEX and PBF-LB/M technologies, Materials (2023) 16.
[47] H. Liu, H. Yu, C. Guo, X. Chen, S. Zhong, L. Zhou, A. Osman et al., Review On Fatigue of Additive Manufactured Metallic Alloys: Microstructure, Performance, Enhancement, and Assessment Methods, Advanced materials (Deerfield Beach, Fla.) 36 (2024) e2306570.
[48] S. Dong, Y. Jiang, J. Dong, F. Wang, W. Ding, Cyclic deformation and fatigue of extruded ZK60 magnesium alloy with aging effects, Mater. Sci. Eng. 615 (2014) 262–272.
[49] L. Nascimento, S.B. Yi, J. Bohlen, D. Letzig, K.U. Kainer, Influence of crystallographic texture on the high cycle fatigue of extruded AZ31 magnesium alloy, MSF 690 (2011) 319–322.
[50] F. Kang, Z. Li, J.T. Wang, P. Cheng, H.Y. Wu, The activation of ⟨c + a⟩ non-basal slip in Magnesium alloys, J. Mater. Sci. 47 (2012) 7854–7859.
[51] J. Victoria-Hernández, S. Yi, D. Letzig, Role of non-basal slip systems on the microstructure and texture development of ZXK-Mg alloy deformed in Plane Strain Compression at elevated temperature, Scr. Mater. 208 (2022) 114322.
[52] Z. Trojanová, P. Lukáč, Compressive deformation behaviour of magnesium alloys, J. Mater. Process. Technol. 162-163 (2005) 416–421.
[53] X. Li, A.G. Sheinerman, Z. Zhu, F. Zhao, Tension-compression asymmetry of grain-boundary sliding: a molecular dynamics study, Mater. Lett. 325 (2022) 132822.
[54] C.M. Cepeda-Jiménez, J.M. Molina-Aldareguia, M.T. Pérez-Prado, Effect of grain size on slip activity in pure magnesium polycrystals, Acta Mater. 84 (2015) 443–456.
[55] H. Somekawa, M. Wakeda, A. Singh, Enhancing ambient temperature grain boundary plasticity by grain refinement in bulk magnesium, Mater. Sci. Eng. 848 (2022) 143424.
[56] G.L. Jia, L.P. Wang, Y.C. Feng, E.J. Guo, Y.H. Chen, C.L. Wang, Microstructure, mechanical properties and fracture behavior of a new WE43 alloy, Rare Met. 40 (2021) 2197–2205.
[57] R. Kumar, M. Mursaleen, G.A. Harmain, Influence of load ratio on fatigue life assessment of AZ31B magnesium alloy under different temperatures, Theor. Appl. Fract. Mech. 133 (2024) 104557.